ARTICLE   OPEN

Check for updates

Thermosteric and dynamic sea level under solar geoengineering

Chao Yue[1], Svetlana Jevrejeva[2], Ying Qu[3,4], Liyun Zhao[1✉] and John C. Moore[5✉]

The IPCC sixth assessment report forecasts sea level rise (SLR) of up to 2 m along coasts by 2100 relative to 1995–2014 following business as usual (SSP585) scenarios. Geoengineering may reduce this threat. We use five Earth System Models simulations of two different solar geoengineering methods (solar dimming and stratospheric sulfate aerosol injection), that offset radiative forcing differences between SSP585 "no-mitigation" and the modest mitigation SSP245 greenhouse gas scenarios, to analyze the impact on global mean thermosteric and dynamic regional sea levels. By 2080–2099, both forms of geoengineering reduce global mean thermosteric sea level by 36–41% (11.2–12.6 cm) relative to SSP585, bringing the global mean SLR under SSP585 in line with that under SSP245, but do not perfectly restore regional SLR patterns. Some of the largest reductions (~18 cm) are on densely populated coasts of eastern Northern America and Japan and along vulnerable Arctic coastal permafrost.

INTRODUCTION

Sea-level rise (SLR) is perhaps the most severe, costly, and irreversible consequence of future global warming[1]. SLR has accelerated from 2.3 (1.6–3.1) mm yr^{-1} during 1971–2018, to 3.7 (3.2–4.2) mm yr^{-1} in 2006–2018, and mean rises of 0.77 (0.63–1.01) m by 2100 are expected under the business-as-usual scenario of the shared socioeconomic pathways[2], with coastlines generally having larger rises[3]. SLR will directly threaten 200 million to 1 billion people living in the low-elevation coastal zone by 2100[4,5], and will pose dire risks to marine coastal ecosystems[2], property values, and infrastructure[6–9]. It is incumbent on science to investigate ways of mitigating, adapting and minimizing the consequences of SLR.

Altering the climate system by increasing the planetary albedo and hence its net radiative balance to mitigate anthropogenic climate warming is a controversial, but increasingly researched topic[10,11], despite grave governance and public acceptability challenges[12,13]. We focus here on the two most widely studied "solar geoengineering" approaches. Solar dimming imposes a decrease in total incoming solar irradiance, while the other, far more plausible method, is stratospheric aerosol injection (SAI). Since solar geoengineering uses short wave radiation to offset longwave forcing, achieving a perfect balance globally is not possible, and because of the vertical differences in atmospheric heating, geoengineered climates are intrinsically drier than greenhouse gas climates[14].

Sea level projections using state-of-the-art Earth System Models (ESMs) have been extensively explored in numerous studies[15,16], but none explicitly examine the response of the sea level to solar geoengineering. In part this is due to the multiplicity of factors that drive changes. Presently, about half of SLR comes from ocean thermal expansion, with a further 44% from the melting of glaciers and ice sheets, and 8% from land-water storage[2]. Each contributor will have a different response to the imposed changes in radiative forcing and the spatial pattern of global temperature changes[17].

A 4 Wm^{-2} radiative forcing reduction, equivalent to e.g., going from Representative Concentration Pathway (RCP) 8.5 to RCP4.5 by solar geoengineering, could lower SLR by 30–40 cm or delay global mean SLR by 40–80 years[18]. Piecemeal studies of SLR in response to geoengineering have been limited to particular elements of the sea level budget, for example the contribution from Greenland[19,20] or raised potential issues due to dynamical impacts on ocean circulation around Antarctica without providing estimates of sea level contributions[21]. The contributions from thermal expansion of ocean water (thermosteric sea level, TSL, "zostoga") and dynamic sea level (DSL, "zos": Methods) fields associated with changes of oceanic currents, and redistributions of ocean heat, salt, and mass to simulations of SLR do not require simulation of mass inputs, and so are well-suited to simulations by ESMs.

In this study, we estimate the global mean TSL and regional DSL during 1995–2099 under the GeoMIP6 (Geoengineering Model Intercomparison Project[22]) G6solar, G6sulfur, and the CMIP6 (Climate Model Intercomparison Project) SSP245 and SSP585 scenarios. The G6 scenarios are not particularly realistic – they begin in 2020, and they consider a background of greenhouse gas emissions that follows the SSP585 scenario, implying no mitigation. They also allow comparison with both the well-known SSP585 that serves as the initial radiative forcing from greenhouse gas emissions, and the moderate emissions SSP245 scenario which serves as the target for net radiative forcing after SAI into the tropical stratosphere (G6sulfur) or solar dimming (G6solar). The only internationally agreed consensus on limiting warming is the Nationally Determined Contributions (NDCs) greenhouse gas emissions framework agreed in Paris in 2015. These NDCs are similar to the trajectory[23] prescribed by the RCP4.5 scenario, which in turn is the previous iteration of SSP245. While SSP585 was designed as a "business as usual" scenario prior to the Paris NDC accords, and should be beyond any reasonable emissions agreements, it represents a large signal to noise ratio, worst-case, scenario. While other scenarios for climate

[1]State Key Laboratory of Earth Surface Processes and Resource Ecology, Faculty of Geographical Science, Beijing Normal University, Beijing, China. [2]National Oceanography Centre, Liverpool, UK. [3]School of Geography Science and Geomatics Engineering, Suzhou University of Science and Technology, Suzhou, China. [4]State Key Laboratory of Cryospheric Science, Northwest Institute of Eco-Environment and Resources, Chinese Academy of Sciences, Lanzhou, China. [5]Arctic Centre, University of Lapland, Rovaniemi, Finland. ✉email: zhaoliyun@bnu.edu.cn; john.moore.bnu@gmail.com
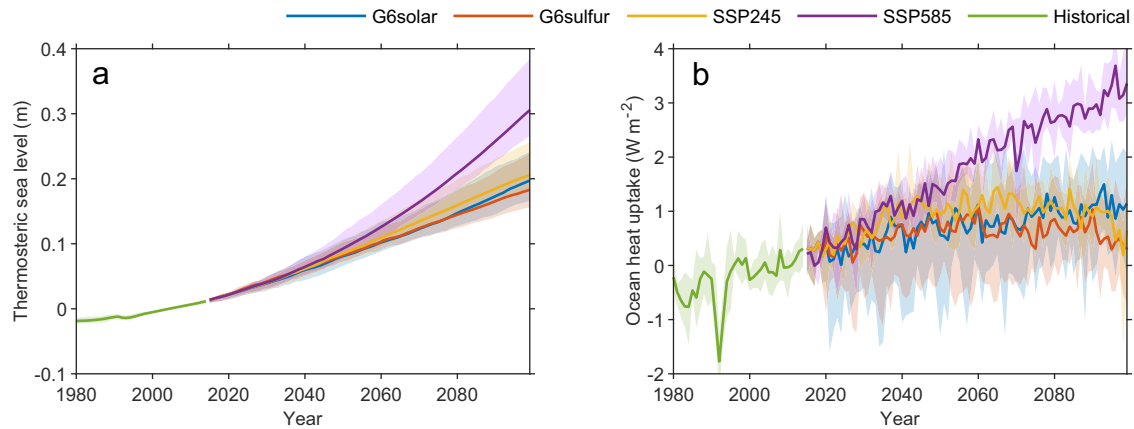
Fig. 1 Global mean thermosteric sea level and ocean heat uptake. Ensemble mean (CNRM-ESM2.1, IPSL-CM6A-LR, MPI-ESM1.2-HR, MPI-ESM1.2-LR, UKESM-1-0-LL) of annual global mean thermosteric sea level (**a**) and ocean heat uptake rate (**b**) from 1980 to 2099 (relative to 1995–2014) under historical, G6solar, G6sulfur, SSP245 and SSP585 scenarios. Shaded areas indicate the across-model spread.

intervention do exist that are arguably more realistic, they have only been run in single models[24]. Hence, the G6 scenarios are most useful to examine across-model variability and utilize the multi-model ensemble to reduce model bias.

SLR under geoengineering scenarios are not simply temperature driven variations on greenhouse has scenarios. Longwave radiative forcing cannot be perfectly offset by reducing shortwave forcing since they differ spatially and on daily and seasonal timescales. Furthermore, known impacts of solar geoengineering include global drying[25], changes in winds[26] and impacts on largescale oceanic transport systems[27] that can both ameliorate greenhouse gas induced changes, or sometimes exacerbate them. Solar dimming simulations are less model dependent than SAI because models have various ways of simulating the stratospheric aerosols (Supplementary table 1), and so G6sulfur temperature and precipitation fields have larger across model differences than those for G6solar[28]. The uncertainties of SLR increase rapidly as temperature rises, driven largely by uncertainties in Antarctic mass loss[3]. Since the primary aim of geoengineering is to lower global temperatures, we may expect that mass contributions to SLR under geoengineering would be both lower, and less uncertain than under pure greenhouse gas climates. Hence, we could expect SLR to be lower everywhere under geoengineering, were it not for regional changes in SLR driven by geoengineering-induced changes in atmospheric and oceanic circulation patterns. Therefore, we aim to answer the following question: How well does solar geoengineering compensate for greenhouse gas driven increases in both global TSL and regional DSL over the 21st century?

RESULTS

Global mean thermosteric sea level projections
Time-varying multi-model ensemble annual mean TSL under the four scenarios (Methods) are shown in Fig. 1a. For the period 1993–2018, the global mean TSL rises by 32.8 ± 4.4 mm (we define uncertainties in this study as the ensemble mean and 95% confidence interval, $N = 5$), which is very close to the observed historical rise in TSL[2] of 32.7 ± 8.9 mm. TSL increases in all scenarios, and shows almost linear trends in SSP245, and the two G6 scenarios. TSL accelerates under SSP585 throughout the 21st century. By the end of this century, the ensemble mean TSL rise is 20.9 ± 2.6 cm for SSP245 and 31.1 ± 4.3 cm for SSP585, which are 0.8 cm and 4.3 cm higher than the mean outputs of 15 CMIP6 ESMs[15]. Under both G6 scenarios, all five ESM reduce the SLR to within 4 cm of SSP245 levels by 2100, and show remarkable decreases compared to SSP585 (Supplementary Table 2). By 2100,

TSL is 11.2 ± 2.1 (12.6 ± 1.7) cm lower under G6solar (G6sulfur) than SSP585, and 1.0 ± 1.2 (2.5 ± 0.9) cm lower than SSP245 (individual ESM results are in Supplementary table 2). Differences of TSL rise in each scenario can be largely attributed to the changes in ocean heat uptake rate, which increases fastest under SSP585 and slowest under G6sulfur (Fig. 1b). These differences are consistent with the effects of the 1991 Pinatubo eruption, often used as a natural analog for SAI[10], which increased atmospheric optical depth and caused ocean heat uptake to decrease dramatically in 1991–92 (Fig. 1b).

Dynamic sea level
We validate ESM simulations of DSL against a 1/12° gridded monthly global ocean reanalysis product that assimilates the altimeter data of TOPEX POSEIDON and ERS-1 satellites (Supplementary Fig. 1), during the historical period of 1995–2014. In general, CMIP6 models have been assessed, and shown to "simulate the mean sea level reasonably well" in comparison with satellite altimetry[29]. The simulated and observed DSL are low in the northern North Atlantic and Southern Ocean due to the formation of the dense North Atlantic Deep Water and the strong Antarctic Circumpolar Current, respectively[29]. DSL is relatively high over subtropical and tropical oceans, especially the western North Pacific Ocean where the DSL is 1 m higher than global mean in both simulations and observations. Multi-model mean DSL is overestimated by 0.13 m globally compared with observations (Supplementary Fig. 1).

Regional sea level
In this study we have used common approach (Methods) to calculate regional sea level by adding the global mean TSL and spatial DSL[2,9,30,31]. Figure 2 shows the first (2020–2039) and last two decades (2080–2099) of the geoengineering period for each scenario. Regional SLR distribution is similar under all scenarios, suggesting that the governing internal processes are relatively similar across each scenario. During the period 2020–2039, SLR is independent of scenario with rises of 4.5 to 4.7 cm. The later period 2080–2099 exhibits scenario-dependent SLR; G6sulfur projects the minimum mean SLR of 16.9 ± 2.2 cm, while the maximum is for SSP585 with mean SLR of 26.0 ± 3.2 cm.

SLR trends during 2020–2100 vary regionally (Fig. 2), with the highest trends over the northern North Atlantic and the northern side of the Southern Ocean. The smallest trends are in the Amundsen Sea. The SSP245 and the two G6 scenarios all project global mean SLR rates of 2.0–2.3 mm yr^{-1}, which are much smaller than 3.4 mm yr^{-1} rate under SSP585 (Fig. 2).
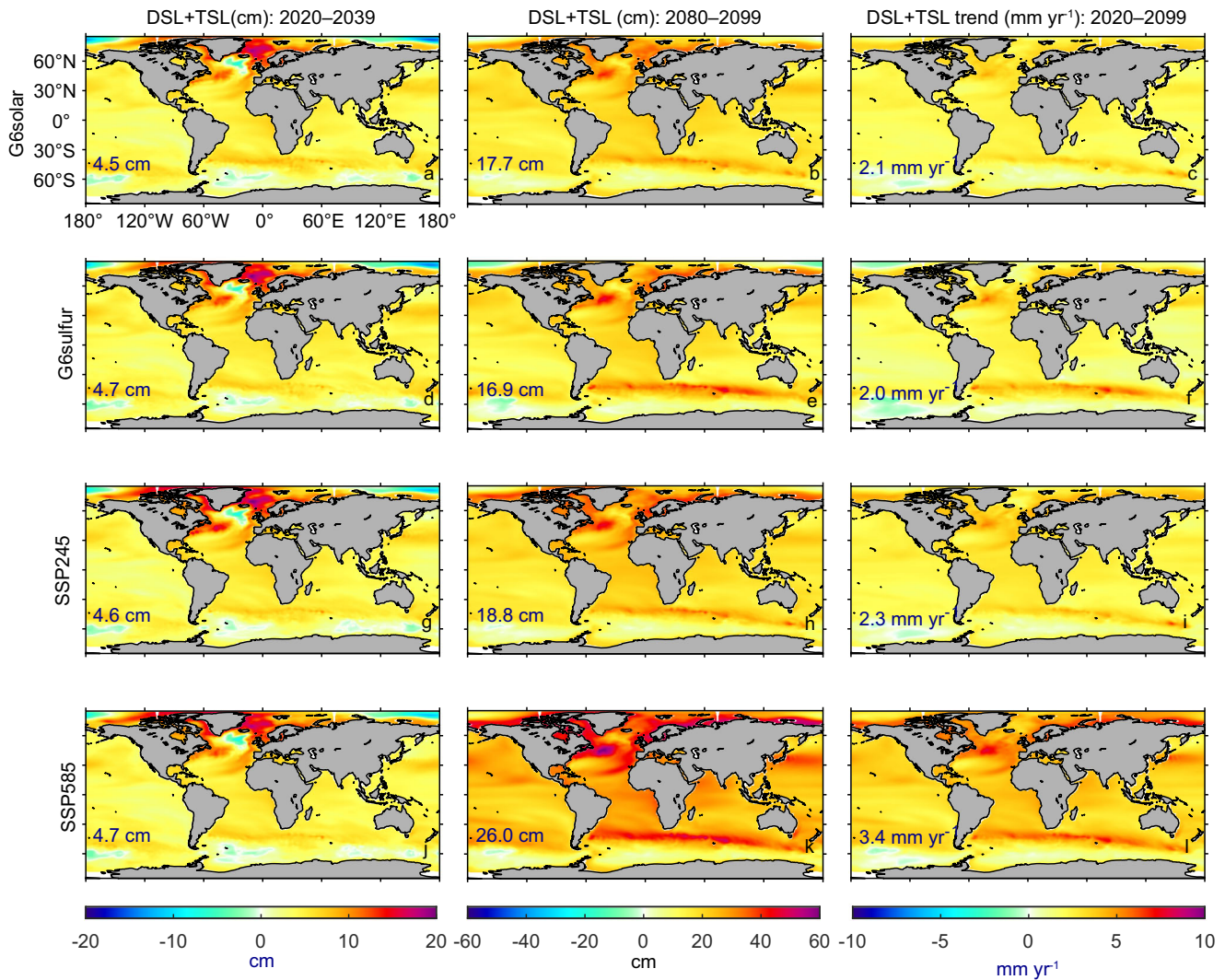
Fig. 2 Multi-model ensemble mean of DSL+TSL. Left column: 2020–2039 and middle column 2080–2099, relative to 1995–2014. Right column shows linear trend. Rows show scenarios from top to bottom: G6solar, G6sulfur, SSP245 and SSP585. The numbers on the bottom left corner of each panel represent the global mean DSL + TSL change for 2020–2039 (left column) and 2080–2099 (middle column) relative to 1995–2014, and the SLR rates during 2020–2100. Individual ESM results are shown in Supplementary Figs. 2–6, and the across model spread indicated in Supplementary Fig. 7.

During 2080–2099, coastal SLR shows largest differences under G6 geoengineering relative to SSP585 in the Arctic Ocean with a trend to smaller differences southward, and even small relative rises at high southern latitudes (Fig. 3, Supplementary Figs. 8–12). Ensemble mean coastal SLR relative to SSP585 is lowered by 0–23 cm under both G6 scenarios, with some of the largest reductions along the densely populated coasts of eastern North America (17.8 ± 5.3 cm) and Japan (18.0 ± 6.4 cm) that are almost double the mean reductions along the global coastline of 9.2 ± 1.0 cm. In the southern hemisphere, G6solar brings the coastal sea level under SSP585 in line with that in SSP245 to within 1 cm or so. G6sulfur, however, performs less well notably along northeastern Japan and southeastern Australia, with sea levels 2–5 cm larger than that under SSP245 (Fig. 3).

Seasonal sea level amplitude can play an important role in local flooding[32,33], and can reveal changes in driving factors, such as seasonal monsoon influences[34]. However, Supplementary Fig. 13 shows that scenario differences in seasonal amplitude are <4 cm everywhere. Differences between G6solar and SSP245 are <1 cm, with the largest coastal differences around the Indonesian Archipelago. There are larger differences (G6sulfur-SSP245),

especially seen in the Southern Ocean and parts of eastern Canada, Vietnam and Japan, and the North Sea, but these changes in seasonal amplitude are about 3 cm. The spatial pattern of the anomalies of G6, especially G6sulfur, with SSP585 appear similar (although opposite in sign) to the mid-latitude seasonal sea surface temperature anomalies between quadrupling CO_2 and pre-industrial control simulations[35]. The seasonal response was attributed to direct CO_2 and wind effects (especially in the southern hemisphere), and that is consistent with the dynamic drivers that we discuss next.

Drivers of dynamic sea level change
Models tend to disagree most where regional SLR is greatest[29], and we find similar effects here. There is large inter-model disagreement for SLR over the Arctic Ocean, and for the overturning regions in the North Atlantic (Supplementary Fig. 7), likely due to considerable model spread in sea ice simulations[36], and the uncertainties in AMOC modeling[37]. DSL spread is also clear in the Southern Ocean, although to lesser degree than for the Arctic and North Atlantic Oceans, presumably due to
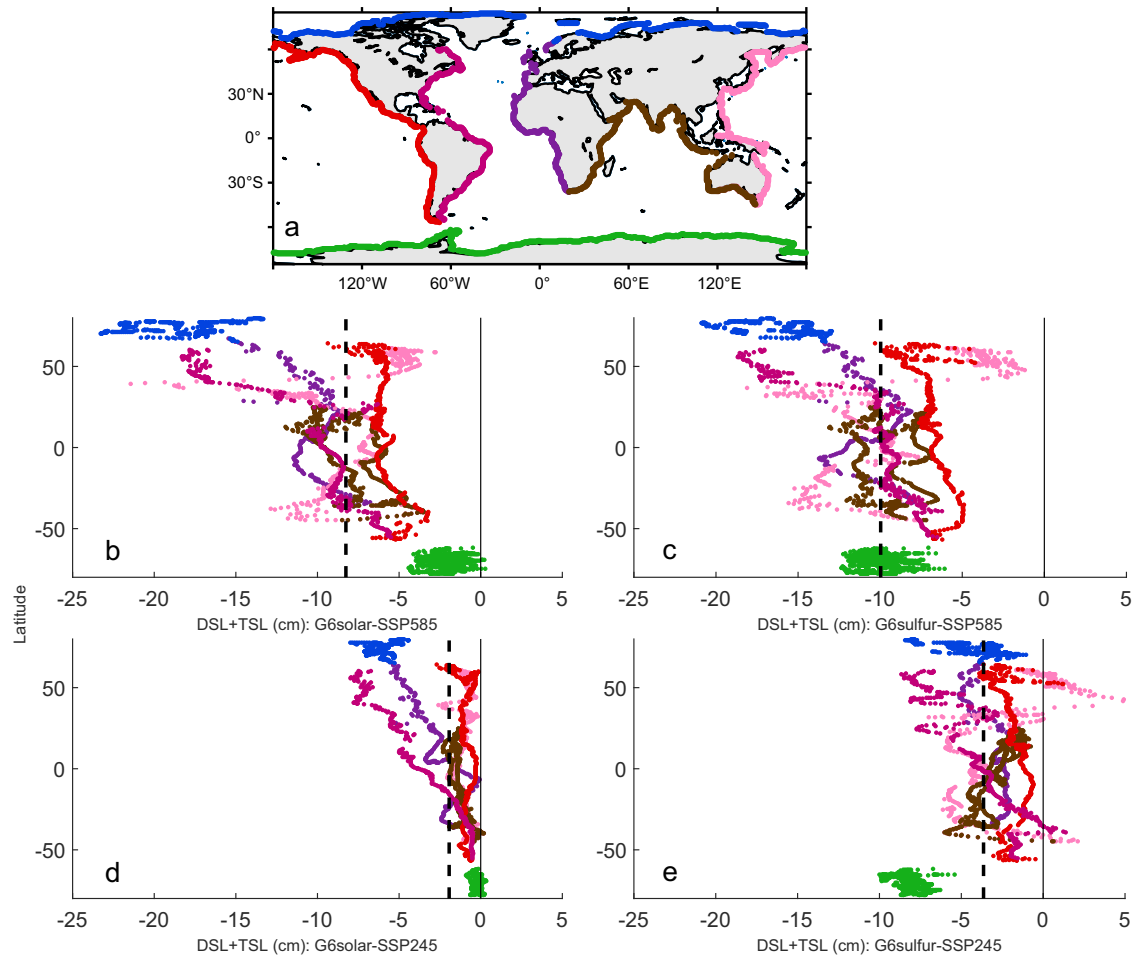
Fig. 3 Coastal sea level rise (SLR). Location map showing color coding of coastal regions (**a**). Five-ESM ensemble mean regional coastal SLR differences of: G6solar–SSP585 (**b**); G6sulfur–SSP585 (**c**); G6solar–SSP245 (**d**); and G6sulfur–SSP245 (**e**) during 2080–2099. Vertical solid lines indicate the zero of coastal sea level rise, thick dashed lines indicate the mean. Individual ESM are shown in Supplementary Figs. 8–12.

simulation differences in the increased westerly wind stress[38], and possibly remotely induced by the weakening of AMOC[37].

There is a significant anticorrelation ($R = -0.83$, $p < 0.01$) between the AMOC and DSL over the North Atlantic (30°N-60°N, 60°W–30°W; Fig. 4e). Under SSP585, SLRs by over 0.5 m in the northern North Atlantic by the end of the century (Fig. 2) due to ocean freshening as Arctic ice melts[39], and the AMOC slowdown is associated with reduced production of deep water[29,40]. The five ESMs simulate AMOC declining by 27–45% of its present-day strength (Supplementary Fig. 19), with declines under SSP585 being largest and those under the two G6 scenarios smallest. Models with the largest present-day simulated AMOC tend to be those that simulate largest future declines[29,41,42], and this is consistent with the behavior of the models studied here.

In the South Atlantic and Indian Ocean sectors of the Southern Ocean, a pattern of increases in sea level from 35°S–55°S between Argentina and New Zealand is obvious under all scenarios by the end of the century (Fig. 2). This is due to increases in wind stress curl and the corresponding change in Sverdrup balance[43], particularly in the Atlantic and Indian ocean sectors of the Southern Ocean[38]. Near the coast of Antarctica, especially west of the Antarctic Peninsula, sea level trends downwards between the early SAI period and the end of the century (Fig. 2 right column). This is related to the strengthening of the Southern Ocean westerlies, particularly in the SSP585 and G6sulfur scenarios (Fig. 4f), which produces a northward Ekman transport flux across the Southern Ocean, as was also noted for earlier greenhouse gas scenarios[44].

Differences due to type of geoengineering

Spatial differences of sea level during 2080–2099 are shown in Fig. 4. Both G6 simulations reduce the SLR relative to SSP585 by 5–25 cm almost everywhere north 50°S. G6sulfur reduces SLR more than G6solar and shows very pronounced reductions both over the Arctic Ocean and eastward of the Australian and Eurasian mid-latitude continents. G6solar, in contrast, shows a more obvious reduction in SLR eastward from mid-latitude South America.

Southern Ocean heat uptake under both G6 scenarios is $3 \pm 1\,\mathrm{W\,m^{-2}}$ less than SSP585. Therefore, the modest SLR predicted there must be a dynamic effect, likely due to the faster Southern Ocean westerlies under SSP585 than G6solar (Fig. 4f), and thus enhanced equatorward Ekman transport under SSP585. There is a significant anticorrelation between the zonal mean of the DSL and westerly wind stress at 60°S ($R = -0.68$, $p < 0.01$; Fig. 4f) under the G6solar, SSP245 and SSP585 scenarios, indicating that the westerly wind stress affects the changes of Southern Ocean sea level. G6sulfur has the strongest westerly wind stress (Fig. 4f) and ocean mass transport (Supplementary Fig. 7) among the scenarios but exhibits a DSL much higher than expected from the regression over the other scenarios (Fig. 4f). This can be explained by the chemical and dynamic effects of SAI on the stratosphere that are absent in the other scenarios. These produce an expanded and deepened southern polar vortex[45] under G6sulfur, helping drive the increased Southern Ocean surface westerly winds.
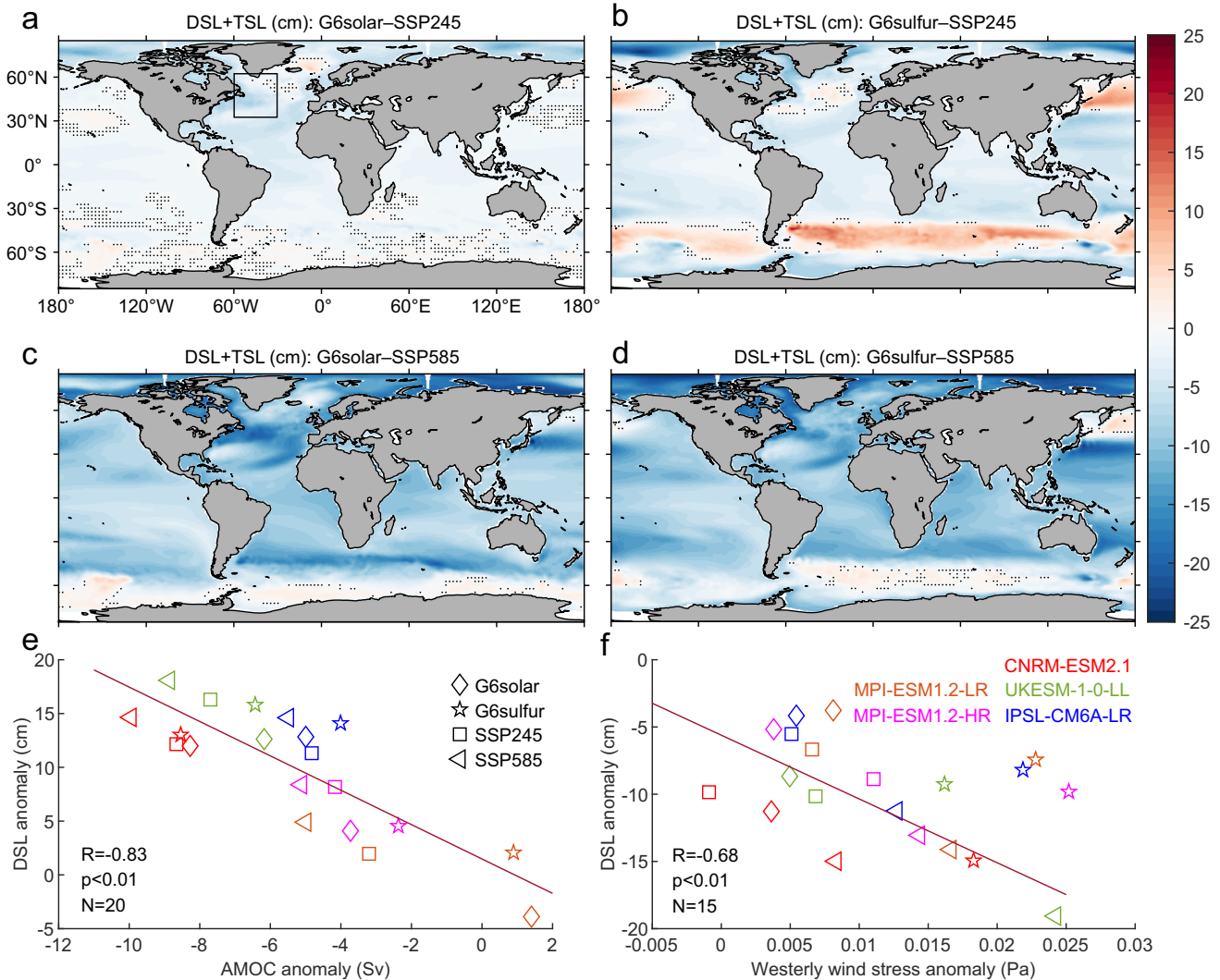
Fig. 4 Regional SLR anomalies and drivers. Five ESM ensemble mean of thermosteric and dynamic SLR differences of (**a**) G6solar-SSP245, (**b**) G6sulfur-SSP245, (**c**) G6solar-SSP585 and (**d**) G6sulfur-SSP585 during 2080–2099 with a common colorbar. Stippling indicates regions with no significant difference at the 95% level by the Wilcoxon sign-rank test. Individual ESM are in Supplementary Figs. 14–18. **e**: regression of DSL in the black box in (**a**) [30°N–60°N, 60°W–30°W] against AMOC index at 30°N relative to 1995–2014 under all scenarios and ESM, with legends in (**e**) and (**f**). **f**: zonal mean DSL versus zonal mean of the westerly wind stress south of 60°S during 2080–2099 relative to 1995–2014, with the regression statistics excluding the G6sulfur scenario (star symbols).

G6sulfur lowers SLR less than G6solar relative to SSP585 in the North Atlantic (Fig. 4c, d), probably due to the correspondingly weaker AMOC in G6sulfur (Fig. 4e, Supplementary Fig. 20), resulting in less deep-water formation, and consequently less regional sea level depression.

Discussion and implications

In our study, we have demonstrated that both G6 simulations are capable of bringing the global mean SLR under SSP585 in line with that under SSP245 (Fig. 1a), which reduce global mean thermosteric sea level by 11.2–12.6 cm relative to rises under SSP585 of 31.1 ± 4.3 cm. Along the global coastline regional, SLR is reduced by 8.6–10.9 cm, with some of the largest changes along the densely populated coasts of eastern Northern America (17.8 ± 5.3 cm) and Japan (18.0 ± 6.4 cm) for both geoengineering scenarios (Fig. 3). These projected reductions of coastal SLR with geoengineering scenarios will reduce the risk of extreme floods in coastal areas, for example, via decreases in the frequency of extreme sea levels associated with tropical and extratropical cyclones in both tropical and high latitude areas[46,47]. Increases in

seasonal amplitude of about 3 cm are simulated in G6sulfur relative to those under both SSP245 and G6solar, but theses seasonal changes are much smaller than the changes in mean SLR under any scenario. Although we have not considered mass increases in our analysis, the so-called fingerprint method[48] allows the TSL and DSL sea level patterns to be adjusted to account for terrestrial ice melt. Mass loss from the ice sheets under geoengineering scenarios has usually considered only changes caused by precipitation differences[19,49], thereby excluding challenging ice dynamical simulations.

Atlantic hurricane flood risk under solar geoengineering is reduced both by lowered risk of large tropical storms, and by lowered rates of SLR[50]. Reduced SLR raises the habitability of low-lying coastlines and moderates financial losses especially in developing nations, where coastal cities are developing fastest and losses represent a larger fraction of wealth[6,9]. The small island states in the developing world are already facing rigorous, in some cases existential, development challenges[51] including increased coastal flooding due to future unmitigated SLR. Coastal flooding damages expected over the 21st century in large coastal

megacities dominate financial losses[52]. For example, the estimated damage from storm Sandy in 2012 to the city of New York is reckoned to have been increased by an additional US $ 2 billion because of the 20 cm SLR over the 20th century[53]. A slower rate of SLR, as simulated under the G6 scenarios would offer more opportunities for graceful adoption of changes in land use planning, particularly for growing cities and small islands[51].

Although costs from urban infrastructure dominate the cost-benefit analysis of SLR[52], there are additional consequences, such as from inundation of low-lying ecosystems. Figure 3 shows the largest sea level reductions in SLR under the G6 scenarios are in the Arctic, which may reflect the Arctic amplifying nature of the climate change response to greenhouse gas forcing[54,55], that is strongly mitigated by the G6 scenarios. Coastal erosion due to permafrost thaw is already threatening the existence of Newtok, Kivalina and other villages in Alaska at enormous per-capita cost to low-income communities[56]. SLR reduces coastal ice-saturated permafrost extent due to the landward migration of the subsurface freshwater-saltwater interface and resulting depression in freezing temperature[57]. For the RCP4.5 scenario, a reduction in SLR of 0.2 cm/yr over the 21st century (comparable to the difference between the G6 and the SSP585 TSL + DSL in the Arctic, Fig. 3) reduces permafrost loss rate by about 15%[57]. Including mass components in total SLR reductions under G6 compared with SSP585 would magnify this difference. Carbon release from Arctic permafrost loss is a significant feedback in future warming scenarios, that can be mitigated by solar geoengineering[58], and the particular pattern of SLR reduction (Fig. 3) would only increase its mitigation value. Myriad other considerations related to geoengineering impacts are of course important, and well beyond the scope of this paper on sea level, but studies have pointed to the potential of geoengineering to moderate key climate hazards and reduce inter-country income inequality[59,60].

The G6 solar geoengineering scenarios do not restore the regional SLR pattern (Fig. 4a, b), particularly in the case of G6sulfur which utilizes SAI, currently thought to be the most realizable and well-studied solar geoengineering option. SAI also produces a different spatial pattern of surface air temperature than the equivalent solar dimming[28]. G6sulfur specifies SAI within the tropical region 10°N–10°S (Supplementary Table 1), and this is a design choice that has both drawbacks and possible benefits over other choices, such as injecting at different seasons and latitudes[61] to target specific impacts from climate warming. Under the G6 scenarios each ESM does not restore sea level to its control state prior to starting geoengineering but rather reflects the perturbed ocean environment that was already impacted by pre-existing greenhouse gas forcing, and this would occur even if net global temperature change was reduced to zero. This means that the models have their own null response, hence using a multi-model ensemble as we have done probably produces a result closer to what the real-world would give, but it also means that the forced response to different types of geoengineering (and greenhouse gases) are blurred and harder to resolve.

Examining the impacts of heat uptake and changing circulation in the system in solar geoengineering scenarios is a useful point of departure for more sophisticated studies exploring mass inputs from melting ice sheets and glaciers, which will be strongly dependent on the solar geoengineering strategy employed. For example, solar geoengineering at high latitudes rather than global solar geoengineering may provide targeted cooling[49], and alternative (or complementary) techniques have also been suggested to minimize mass loss from melting ice[62]. Furthermore, the realizations available in G6 scenarios are few and hence extracting climate signal from stochastic noise in each model is difficult. Details of the climate response would be strengthened by more model groups committing to running newer scenarios such as the multi-latitude injection feedback simulations designed to stabilize temperatures at 1.5° or 2 °C above pre-industrial using SAI

with more ensemble members[24], or more localized approaches such as marine cloud brightening[22].

DSL projections are critically affected by wind stress, model resolution, and parameterization. There are large uncertainties in simulating DSL for different scenarios and by different models as has previously been discussed[2,63]. CMIP6 ESM, as with their CMIP5 counterparts, show disagreement in projecting DLS changes particularly over the North Atlantic and Southern Ocean[29,64], but nevertheless do represent an improvement[65]. The North Atlantic is influenced by dynamic changes to AMOC circulation, while the Southern Ocean is expected to experience largest increases in surface winds. Furthermore, the AMOC change may also impacts the Southern Ocean[37]. Both G6solar and G6sulfur affect AMOC in essentially the same way as the pure GHG scenarios as evidenced by all scenarios falling on the same regression line in Fig. 4e. In the south, G6sulfur stands apart from the other scenarios (Fig. 4f), probably because of the larger impact of aerosols on the southern polar vortex[45] and the zonally unconfined Southern Ocean. However, other possibilities also exist such as hemispheric differences in polar amplification[55], sea ice feedbacks[66], and the impacts of greenhouse gases on tropospheric circulation[67]. Understanding these high latitude mechanisms under both increasing greenhouse gases and short wave balancing under solar geoengineering will be increasingly important in future.

METHODS

We utilize two scenarios from the CMIP6 suite of simulations: SSP245 is a medium emissions scenario with radiative forcing peaking in mid-century and global mean temperatures rising relatively slowly until well after 2100; SSP585 is a no-mitigation emissions scenario with radiative forcing rising throughout the century[68]. We use two solar geoengineering scenarios from GeoMIP6: G6solar takes SSP585 as the greenhouse gas scenario but imposes a reduction in solar constant to return net forcing to match SSP245 from 2020–2099, while G6sulfur is similar but uses SAI of sulfate aerosols into the near-equatorial lower stratosphere instead of solar dimming to reduce net forcing to SSP245[69]. The G6 scenarios are useful because they have been done by six CMIP6 generation ESMs[28], five of which have sea level data fields available (Supplementary Table 1).

We calculate the monthly TSL and DSL during 1993–2099 from all five CMIP6 generation ESMs that have the relevant data fields available from the GeoMIP scenarios: CNRM-ESM2.1, IPSL-CM6A-LR, MPI-ESM1.2-HR, MPI-ESM1.2-LR, UKESM-1.0-LL (Supplementary Table 1). Climate projections based on ESMs are strongly influenced by the equilibrium climate sensitivity (ECS), which explicitly describes the global mean temperature increase associated with a doubling of atmospheric carbon dioxide. The mean ECS of ESM used in this study is 4.3 ± 0.9 °C (Supplementary Table 1), slightly higher than a 38 CMIP6 model ensemble mean of 3.7 ± 1.1 °C[70].

We used a well-developed method for calculations of TSL and DSL, that has been adopted for the IPCC sea level projection and is suitable for output from models under CMIP standard, including GeoMIP. TSL and DSL are specific variables available from the CMIP type model simulations, named as "zostoga" and "zos" respectively. Full description for the variable calculations is available from Appendix H7 (zos) and Appendix H9 (zostoga) in ref. [31]. This approach and use of the zos and zostoga variables has been utilized in numerous publications about sea level projections, e.g., IPCC AR6 regional sea level projections[2,3,30,71]. We corrected ESMs for drifts in both TSL and DSL using the standard "linear drift correction"[72] and inverse barometer effects[3] to equivalent sea level. We account for the fact that some of the models employ the Boussinesq approximation (mass conserving) whilst others do not (volume conserving), by calculating the global mean signal from each time slice and remove it at each grid

point for that time slice. We bi-linearly interpolated each ESM to a common grid of $0.5° \times 0.5°$ resolution to facilitate multi-model ensemble mean calculation. We do not consider contribution to SLR from ice mass losses from glaciers and ice sheets, the smaller contributions expected in land-water storage, or vertical land motion.

We focus on the drivers for regional sea level variability such as the surface zonal wind stress, and the Atlantic and Southern Ocean Meridional Overturning Circulation (AMOC; SMOC). We define AMOC and SMOC strength here as the maximum overturning stream function over the Northern Atlantic at 30°N, and over the Southern Ocean at 60°S, respectively.

DATA AVAILABILITY
GeoMIP and CMIP6 data are available on the Earth System Grid Federation (https://esgf-node.llnl.gov/).

CODE AVAILABILITY
The data analysis and figure drawing computer codes are in Matlab and NCAR Command Language (NCL) scripts and are available from the authors upon reasonable request.

REFERENCES
1. Hauer, M. E. et al. Sea-level rise and human migration. *Nat. Rev. Earth Environ.* **1**, 28–39 (2020).
2. Fox-Kemper, B. et al. Ocean, Cryosphere and sea level change. In: Climate Change 2021: The physical science basis. Contribution of Working Group I to the Sixth Assessment Report of the Intergovernmental Panel on Climate Change. Cambridge University Press (2021).
3. Jevrejeva, S., Jackson, L. P., Riva, R. E. M., Grinsted, A. & Moore, J. C. Coastal sea level rise with warming above 2 C. *Proc. Natl. Acad. Sci. USA* **113**, 13342–13347 (2016).
4. Kirezci, E. et al. Projections of global-scale extreme sea levels and resulting episodic coastal flooding over the 21st Century. *Sci. Rep.* **10**, 11629 (2020).
5. Neumann, B., Vafeidis, A. T., Zimmermann, J. & Nicholls, R. J. Future coastal population growth and exposure to sea-level rise and coastal flooding-a global assessment. *PLoS One* **10**, e0118571 (2015).
6. Brown, S. et al. Global costs of protecting against sea-level rise at 1.5 to 4.0 °C. *Clim. Change* **167**, 1–21 (2021).
7. Keenan, J. M., Hill, T. & Gumber, A. Climate gentrification: from theory to empiricism in Miami-Dade County, Florida. *Environ. Res. Lett.* **13**, 54001 (2018).
8. Fussell, E. et al. Weather-related hazards and population change: a study of hurricanes and tropical storms in the United States, 1980–2012. *Ann. Am. Acad. Political Soc. Sci.* **669**, 146–167 (2017).
9. Jevrejeva, S., Jackson, L. P., Grinsted, A., Lincke, D. & Marzeion, B. Flood damage costs under the sea level rise with warming of 1.5 C and 2 C. *Environ. Res. Lett.* **13**, 74014 (2018).
10. Shepherd, J. G. *Geoengineering the climate: science, governance and uncertainty* (Royal Society), London (2009).
11. Keith, D. W. Toward constructive disagreement about geoengineering. *Science* **374**, 812–815 (2021).
12. MacNaghten, P. & Owen, R. Good governance for geoengineering. *Nature* **479**, 293 (2011).
13. McLaren, D. & Corry, O. The politics and governance of research into solar geoengineering. *Wiley Interdiscip. Rev. Clim. Chang* **12**, e707 (2021).
14. Govindasamy, B., Caldeira, K. & Duffy, P. B. Geoengineering Earth's radiation balance to mitigate climate change from a quadrupling of CO2. *Glob. Planet. Change* **37**, 157–168 (2003).
15. Jevrejeva, S., Palanisamy, H. & Jackson, L. P. Global mean thermosteric sea level projections by 2100 in CMIP6 climate models. *Environ. Res. Lett.* **16**, 14028 (2020).
16. Palmer, M. D. et al. Exploring the drivers of global and local sea-level change over the 21st century and beyond. *Earth's Futur.* **8**, e2019EF001413 (2020).
17. Irvine, P. J., Keith, D. W. & Moore, J. C. Brief communication: understanding solar geoengineering's potential to limit sea level rise requires attention from cryosphere experts. *Cryosphere* **12**, 2501–2513 (2018).
18. Moore, J. C., Jevrejeva, S. & Grinsted, A. Efficacy of geoengineering to limit 21st century sea-level rise. *Proc. Natl. Acad. Sci. USA* **107**, 15699–15703 (2010).
19. Moore, J. C. et al. Greenland ice sheet response to stratospheric aerosol injection geoengineering. *Earth's Futur* **7**, 1451–1463 (2019).
20. Fettweis, X. et al. Brief communication: reduction in the future Greenland ice sheet surface melt with the help of solar geoengineering. *Cryosphere* **15**, 3013–3019 (2021).
21. McCusker, K. E., Battisti, D. S. & Bitz, C. M. Inability of stratospheric sulfate aerosol injections to preserve the West Antarctic ice sheet. *Geophys. Res. Lett.* **42**, 4989–4997 (2015).
22. Visioni, D. et al. Opinion: The scientific and community-building roles of the Geoengineering Model Intercomparison Project (GeoMIP) – past, present, and future. *Atmos. Chem. Phys.* **23**, 5149–5176 (2023).
23. Kitous, A., & Keramidas, K. Analysis of scenarios integrating the INDCs. JRC97845 Eur. Comm. (2015).
24. MacMartin, D. G. et al. Scenarios for modeling solar radiation modification. *Proc. Natl. Acad. Sci. USA* **119**, e2202230119 (2022).
25. Bala, G., Duffy, P. B. & Taylor, K. E. Impact of geoengineering schemes on the global hydrological cycle. *Proc. Natl. Acad. Sci. USA.* **105**, 7664–7669 (2008).
26. Gertler, C. G. et al. Weakening of the extratropical storm tracks in solar geoengineering scenarios. *Geophys. Res. Lett.* **47**, e2020GL087348 (2020).
27. Xie, M., Moore, J. C., Zhao, L., Wolovick, M. & Muri, H. Impacts of three types of solar geoengineering on the Atlantic Meridional overturning circulation. *Atmos. Chem. Phys.* **22**, 4581–4597 (2022).
28. Visioni, D. et al. Identifying the sources of uncertainty in climate model simulations of solar radiation modification with the G6sulfur and G6solar Geoengineering Model Intercomparison Project (GeoMIP) simulations. *Atmos. Chem. Phys.* **21**, 10039–10063 (2021).
29. Lyu, K., Zhang, X. & Church, J. A. Regional dynamic sea level simulated in the CMIP5 and CMIP6 models: mean biases, future projections, and their linkages. *J. Clim.* **33**, 6377–6398 (2020).
30. Kopp, R. E. et al. Probabilistic 21st and 22nd century sea-level projections at a global network of tide-gauge sites. *Earth's Future* **2**, 383–406 (2014).
31. Griffies, S. M. et al. OMIP contribution to CMIP6: experimental and diagnostic protocol for the physical component of the ocean model intercomparison project. *Geosci. Model Dev.* **9**, 3231–3296 (2016).
32. Wahl, T., Calafat, F. M. & Luther, M. E. Rapid changes in the seasonal sea level cycle along the US Gulf coast from the late 20th century. *Geophys. Res. Lett.* **41**, 491–498 (2014).
33. Amiruddin, A. M. et al. The seasonal cycle and variability of sea level in the South China Sea. *J. Geophys. Res.* **120**, 5490–5513 (2015).
34. Qu, Y., Jevrejeva, S., Williams, J. & Moore, J. C. Drivers for seasonal variability in sea level around the China seas. *Glob. Planet. Change* **213**, 103819 (2022).
35. Liu, F., Lu, J., Luo, Y., Huang, Y. & Song, F. On the oceanic origin for the enhanced seasonal cycle of SST in the midlatitudes under global warming. *J. Clim.* **33**, 8401–8413 (2020).
36. Berdahl, M. et al. Arctic cryosphere response in the geoengineering model intercomparison project G3 and G4 scenarios. *J. Geophys. Res. Atmos.* **119**, 1308–1321 (2014).
37. Chen, C., Liu, W. & Wang, G. Understanding the uncertainty in the 21st century dynamic sea level projections: the role of the AMOC. *Geophys. Res. Lett.* **46**, 210–217 (2019).
38. Bouttes, N., Gregory, J. M., Kuhlbrodt, T. & Suzuki, T. The effect of windstress change on future sea level change in the Southern Ocean. *Geophys. Res. Lett.* **39** https://doi.org/10.1029/2012GL054207 (2012).
39. Munk, W. Ocean freshening, sea level rising. *Science* **300**, 2041–2043 (2003).
40. Levermann, A., Griesel, A., Hofmann, M., Montoya, M. & Rahmstorf, S. Dynamic sea level changes following changes in the thermohaline circulation. *Clim. Dyn.* **24**, 347–354 (2005).
41. Cheng, W., Chiang, J. C. H. & Zhang, D. Atlantic meridional overturning circulation (AMOC) in CMIP5 models: RCP and historical simulations. *J. Clim.* **26**, 7187–7197 (2013).
42. Hong, Y. et al. Impact of the GeoMIP G1 sunshade geoengineering experiment on the Atlantic meridional overturning circulation. *Environ. Res. Lett.* **12**, 34009 (2017).
43. Sverdrup, H. U. Wind-driven currents in a baroclinic ocean; with application to the equatorial currents of the eastern Pacific. *Proc. Natl. Acad. Sci. USA* **33**, 318 (1947).
44. Yin, J., Griffies, S. M. & Stouffer, R. J. Spatial variability of sea level rise in twenty-first century projections. *J. Clim.* **23**, 4585–4607 (2010).
45. Visioni, D. et al. Reduced poleward transport due to stratospheric heating under stratospheric aerosols geoengineering. *Geophys. Res. Lett.* **47**, e2020GL089470 (2020).
46. Vitousek, S. et al. Doubling of coastal flooding frequency within decades due to sea-level rise. *Sci. Rep.* **7**, 1–9 (2017).

47. Vousdoukas, M. I. et al. Global probabilistic projections of extreme sea levels show intensification of coastal flood hazard. *Nat. Commun.* **9**, 1–12 (2018).

48. Jackson, L. P. & Jevrejeva, S. A probabilistic approach to 21st century regional sea-level projections using RCP and High-end scenarios. *Glob. Planet. Change* **146**, 179–189 (2016).

49. Lee, W. R. et al. High-latitude stratospheric aerosol injection to preserve the Arctic. *Earth's Future* **11**, e2022EF003052 (2023).

50. Moore, J. C. et al. Atlantic hurricane surge response to geoengineering. *Proc. Natl. Acad. Sci. USA* **112**, 13794–13799 (2015).

51. Oppenheimer, M. et al., Sea level rise and implications for low lying islands, coasts and communities, IPCC Special Report on the Ocean and Cryosphere in a Changing Climate (2019).

52. Abadie, L. M., Jackson, L. P., de Murieta, E. S., Jevrejeva, S. & Galarraga, I. Comparing urban coastal flood risk in 136 cities under two alternative sea-level projections: RCP 8.5 and an expert opinion-based high-end scenario. *Ocean Coast. Manag.* **193**, 105249 (2020).

53. Leifert, H. Sea level rise added $2 billion to Sandy's toll in New York City. *Eos* **96**, 16 (2015).

54. Walsh, J. E. Intensified warming of the arctic: causes and impacts on middle latitudes. *Glob. Planet. Chang.* **117**, 52–63 (2014).

55. Chemke, R. & Polvani, L. M. Linking midlatitudes eddy heat flux trends and polar amplification. *npj Clim. Atmos. Sci.* **3**, 1–8 (2020).

56. Guardian. https://www.theguardian.com/environment/interactive/2013/may/14/alaska-villages-frontline-global-warming (2013).

57. Guimond, J. A., Mohammed, A. A., Walvoord, M. A., Bense, V. F. & Kurylyk, B. L. Saltwater intrusion intensifies coastal permafrost thaw. *Geophys. Res. Lett.* **48**, e2021GL094776 (2021).

58. Chen, Y., Liu, A. & Moore, J. C. Mitigation of Arctic permafrost carbon loss through stratospheric aerosol geoengineering. *Nat. Commun.* **11**, 1–10 (2020).

59. Irvine, P., et al. Halving warming with idealized solar geoengineering moderates key climate hazards. Nat. Clim. Chang *9*. https://doi.org/10.1038/s41558-019-0398-8 (2019).

60. Harding, A. R., Ricke, K., Heyen, D., MacMartin, D. G., and Moreno-Cruz, J. Climate econometric models indicate solar geoengineering would reduce inter-country income inequality. Nat. Commun. *11*. https://doi.org/10.1038/s41467-019-13957-x. (2020).

61. Kravitz, B. et al. The Geoengineering Model Intercomparison Project Phase 6 (GeoMIP6): Simulation design and preliminary results. *Geosci. Model Dev.* **8**, 3379–3392 (2015).

62. Wolovick, M. J. & Moore, J. C. Stopping the flood: could we use targeted geoengineering to mitigate sea level rise? *Cryosphere* **12**, 2955–2967 (2018).

63. van de Wal RSW X. Zhang, et al, Uncertainties in long-term twenty-first century process-based coastal sea-level projections. *Surv. Geophys.* https://doi.org/10.1007/s10712-019-09575-3 (2019).

64. Little, C. M., Horton, R. M., Kopp, R. E., Oppenheimer, M. & Yip, S. Uncertainty in twenty-first-century CMIP5 sea level projections. *J. Clim.* **28**, 838–852 (2015).

65. Beadling, R. L. et al. Representation of Southern ocean properties across Coupled Model Intercomparison Project Generations: CMIP3 to CMIP6. *J. Clim.* **33**, 6555–6581 (2020).

66. Li, H. & Fedorov, A. V. Persistent freshening of the Arctic Ocean and changes in the North Atlantic salinity caused by Arctic sea ice decline. *Clim. Dyn.*, 1–19 https://doi.org/10.1007/s00382-021-05850-5 (2021).

67. Grise, K. M. et al. Recent tropical expansion: natural variability or forced response? *J. Clim.* **32**, 1551–1571 (2019).

68. O'Neill, B. C. et al. The scenario model intercomparison project (ScenarioMIP) for CMIP6. *Geosci. Model Dev.* **9**, 3461–3482 (2016).

69. Kravitz, B., MacMartin, D. G., Wang, H. & Rasch, P. J. Geoengineering as a design problem. *Earth Syst. Dynam.* **7**, 469–497 (2016).

70. Meehl, G. A. et al. Context for interpreting equilibrium climate sensitivity and transient climate response from the CMIP6 Earth system models. *Sci. Adv.* **6**, eaba1981 (2020).

71. Garner, G. G. et al. IPCC AR6 WGI Sea Level Projections. (2022).

72. Sen Gupta, A., Jourdain, N. C., Brown, J. N. & Monselesan, D. Climate Drift in the CMIP5 Models. *J. Clim.* 8597–8615 https://doi.org/10.1175/JCLI-D-12-00521.1 (2013).

AUTHOR CONTRIBUTIONS

C.Y., J.C.M. and S.J. conceived the research. C.Y. processed model results and prepared graphics. C.Y., J.C.M. and S.J. interpreted the results. C.Y., J.C.M. and S.J. prepared the draft. All authors discussed and commented on the outcome.

COMPETING INTERESTS

The authors declare no competing interests.

ADDITIONAL INFORMATION

Supplementary information The online version contains supplementary material available at https://doi.org/10.1038/s41612-023-00466-4.

Correspondence and requests for materials should be addressed to Liyun Zhao or John C. Moore.

Reprints and permission information is available at http://www.nature.com/reprints

Publisher's note Springer Nature remains neutral with regard to jurisdictional claims in published maps and institutional affiliations.